Journal of Radiation Research and Applied Sciences 18 (2025) 101976

Contents lists available at ScienceDirect

Journal of Radiation Research and Applied Sciences

journal homepage: www.journals.elsevier.com/journal-of-radiation-research-and-applied-sciences

Heavy metals and radioactivity assessment of the coastal sediments at Abu Ghusun, southern Red Sea, Egypt

Ahmed Abdelaal [a], Gehad M. Saleh [b], El Saeed R. Lasheen [c,*], Mabrouk Sami [d], Farrage M. Khaleal [b], Ioan V. Sanislav [e], Fathy Abdalla [f,**]

[a] Environmental Sciences Department, Faculty of Science, Port Said University, Port Said, 42522, Egypt
[b] Nuclear Materials Authority, P. O. Box 530, El-Maadi, Cairo, Egypt
[c] Geology Department, Faculty of Science, Al-Azhar University, Cairo, Egypt
[d] Geosciences Department College of Science United Arab Emirates University, 15551, Al Ain, United Arab Emirates
[e] Economic Geology Research Centre (EGRU), College of Science and Engineering, James Cook University, Townsville, QLD, 4811, Australia
[f] College of Science, King Saud University, Riyadh, 11451, Saudi Arabia

ARTICLE INFO

Keywords:
Heavy metals
Radiation
Ecological indices
Red sea

ABSTRACT

Coastal sediments act as both sinks and secondary sources of pollutants, making their assessment essential for understanding ecological and human health risks in sensitive marine environments. This study evaluated the concentrations of nine trace metals and natural radionuclides in surface sediments from Abu Ghusun, south Red Sea to assess their ecological, radiological, and health implications. Sediment texture, organic matter, and metal concentrations were analyzed, followed by application of international sediment quality guidelines and multiple ecological risk indices. The results showed that Pb, Cr, Ba, Cu, and Ni exceeded the Effect Range Median (ERM) thresholds, suggesting potential adverse effects on benthic organisms. Cr and V also surpassed Canadian soil quality guidelines and global upper crust values. Enrichment Factor analysis indicated significant enrichment of Pb and Ni, while contamination indices revealed considerable to elevated contamination for most metals, particularly Zn and Pb. Geo-accumulation (I_{geo}) values > 5 identified areas of severe contamination. Despite this, the Potential Ecological Risk Index (PERI) indicated low ecological threat (<150), though the mean ERM quotient suggested a medium–high priority risk. Toxicological risk assessment showed moderate toxicity potential, while human health evaluation revealed negligible non-carcinogenic and carcinogenic risks. The activity concentrations of ^{232}Th (12.1 ± 6.42 Bq/kg), ^{226}Ra (24.53 ± 5.65 Bq/kg), and ^{40}K (337.06 ± 64.98 Bq/kg) were below gobal safety limits, indicating no radiological hazards. This study offers the first integrated assessment of trace metals and radionuclides in Abu Ghusun sediments, combining ecological, radiological, and health risk indices to reveal localized Pb, Ni, and Zn enrichment. Continuous monitoring is recommended to track pollutant inputs, particularly from anthropogenic activities. Remediation strategies and stricter regulation of potential metal sources should be implemented to protect the Red Sea ecosystem.

1. Introduction

Heavy metals have increased globally as a result of farming, manufacturing, and urbanization (Abdelaal et al., 2024; Lasheen et al., 2025; Saleh, Lasheen, et al., 2025; Vaezi & Lak, 2023). These metals pose serious risks to living organisms because they are persistent, difficult to remove, and tend to accumulate in aquatic and terrestrial environments, ultimately threatening ecosystems and human health (Zhao et al., 2023). Continuous monitoring is therefore essential to mitigate their impacts (Ardila et al., 2023). Sediments in Simenit and Akgöl Lakes, Turey show moderate–high contamination from Cr, Ni, and Cd, mainly from industrial and agricultural sources, posing ecological and child health risks (Yüksel et al., 2025) (see Table 2).

The Red Sea coastal areas are strongly influenced by geological processes such as erosion and deposition (Al-Kahtany et al., 2023). However, rapid growth of tourism and coastal development in Egypt has placed pressure on coral reef ecosystems and nearshore sediments. Several studies have examined heavy metal contamination in Red Sea

* Corresponding author.
** Corresponding author.
E-mail addresses: elsaeedlasheen@azhar.edu.eg (E.S.R. Lasheen), Fabdalla@ksu.edu.sa (F. Abdalla).

https://doi.org/10.1016/j.jrras.2025.101976
Received 13 August 2025; Received in revised form 26 August 2025; Accepted 20 September 2025
Available online 27 September 2025

sediments, focusing on their distribution and chemical forms (Al-Mur et al., 2025; Lasheen et al., 2024, 2025). Understanding the sources of these contaminants is vital for effective environmental management. To achieve this, a range of ecological indices—such as the pollution load index, contamination and geo-accumulation factors, and sediment quality guidelines—have been applied, along with human health risk assessments including hazard quotients and cancer risk evaluations (Lasheen, Mansour, et al., 2024; Mohammadi et al., 2019).

The Red Sea is not only one of the world's most important commercial routes but also a region of high ecological and economic value. It serves as a source of oil, fisheries, and tourism revenues, while its beaches contain heavy mineral deposits such as rutile, garnet, and ilmenite (Khaleal et al., 2023). These resources, however, may also introduce environmental risks when eroded from surrounding rocks. Anthropogenic activities including recreation, fishing, landfill, and industrial discharges are additional contributors to sediment pollution. The expansion of resorts and other infrastructure along Egypt's Red Sea coast has accelerated ecological stress, highlighting the urgent need for coral reef protection and sustainable management strategies (Reeves, 1977; Al-Mur et al., 2025).

Alongside heavy metal pollution, natural radioactivity in sediments represents another environmental concern. Radionuclides such as ^{40}K,

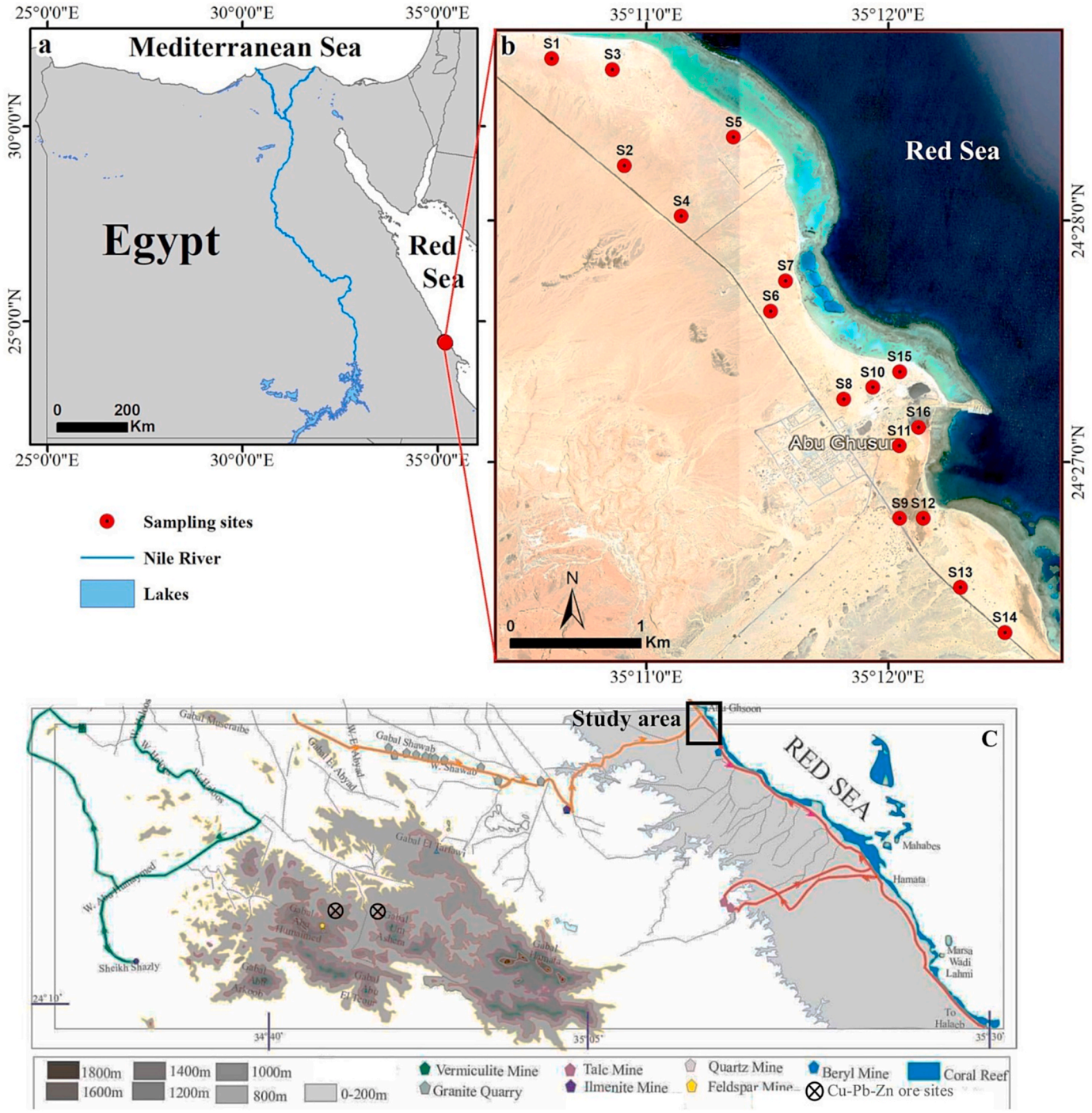

Fig. 1. a) Abu Ghusun area map, Red Sea, South Egypt. b) 6, 5, 6 bands prevailing sampling sites. c) Simplified topographic map showing the geological features (e.g., G. Shawab and G. Hamata) and mining/ore sites (e.g., Cu-Pb-Zn-Ag ores, vermiculite, granite, talc, ilmenite, and beryl) of Wadi Shawab at about 30–50 km.

^{226}Ra, and ^{232}Th are naturally occurring in rocks and soils, with concentrations influenced by geology, soil type, and topography (Freitas & Alencar, 2004; Kumar et al., 2024; UNSCEAR, 2010). In the Red Sea, erosion and transport of zircon- and xenotime-rich sediments may increase uranium and thorium levels. Long-term exposure to radionuclides poses health risks, including cancers and damage to bones, kidneys, and the respiratory system (Hanfi et al., 2022; Zakaly et al., 2024). Therefore, assessing the radiological hazards in sediments is essential for evaluating potential risks to both ecosystems and human populations.

This research represents the first integrated assessment of heavy metal contamination and natural radioactivity in the sediments of Abu Ghusun, southern Egypt, along the Red Sea. The sediments in this area are of economic importance for tourism, infrastructure, and even potential nuclear industry use. Specifically, this study aims to: 1) Apply correlation factors, ecological indices, and health risk assessments to evaluate potential hazards for both adults and children through direct contact with sediments, 2) Utilize GIS-based spatial analysis to map the distribution of heavy metals, 3) Assess the radiological risks of ^{40}K, ^{226}Ra, and ^{232}Th in sediments using exposure and dose-based indices (absorbed gamma dose, annual effective dose, radium equivalent activity, and gonadal dose), and 4) Provide baseline data to guide management strategies aimed at mitigating heavy metal and radiological risks. This study emphasizes the critical need for comprehensive monitoring and management of sediment quality along the Red Sea, ensuring the protection of marine ecosystems, human health, and the long-term sustainability of coastal resources. While some studies have addressed heavy metals or radionuclides separately in Red Sea sediments, no integrated assessment combining ecological, human health, and radiological risks has been conducted for Abu Ghusun area, this study fills a critical gap in understanding the cumulative environmental threats in this region.

2. Material and methodology

2.1. Geology of Abu Ghusun area

Abu Ghusun area, lie on the Red Sea coastline in Egypt (Fig. 1a), is part of the extreme southern Egyptian Eastern Desert (Lasheen et al., 2025; Saleh, Kamar, et al., 2025). The Eastern Desert is characterized by Nubian crystalline rocks with variable age, color, texture, petrogenesis, and dynamic setting (Lasheen, Sami, et al., 2024). Abu Ghusun boasts a distinctive geological environment defined by its specific lithofacies and sedimentary history. This area is a component of the Ras Banas Peninsula (Fig. 1b), which showcases two primary rock formations dating from the Oligocene to Lower Middle Miocene epochs: the Abu Ghusun and Um Mahara Formations (Mohammed et al., 2024). Stretching approximately 50 km, the Ras Banas Peninsula is marked by Precambrian basement rocks on its southwestern edge and sedimentary rocks on its northeastern side. The basement rocks form hill chains and likely constituted a submarine elevation prior to the deposition of Miocene rocks. Landsat-8 OLI satellite image has been utilized to land/water features in the region, (Fig. 1b). In order to delineate the land use features of the research area, a composite bands instruments has been fitted to the OLI image utilizing bands (6, 5, and 6). (Fig. 1b) (Saralioglu & Vatandaslar, 2022). The sediments consist of a wide range of textural classes, with sand being the predominant component of beach areas (Figs. S1a, b, and c). Sand is covered with gravel in some parts. Mangrove swamps are widely distributed along the shoreline, producing leaves and organic debris that improves mangrove swamps and spreads to neighboring areas (Fig. S1d). The exterior shape, unique layout, and orientation of different sand dunes can distinguish them from one another.

2.2. Sediment's sampling and analysis

Abu Ghusun lagoon, which extends approximately 1.5 km along the Red Sea coast and is about 300 m wide, with depths reaching up to 6 m at high tide (Fig. 1b). Using a hand auger, researchers extracted 16 sediment samples (S1-16) of the Abu Ghusun region, Red Sea coast (Fig. 1b) in June 2023 because this period corresponds to the dry summer season along the Red Sea, when wadi flux and rainfall-driven dilution are minimal, ensuring that the measured heavy metal and radionuclide concentrations reflect stable baseline conditions and not short-term seasonal variability. Sediments samples were collected in the onshore coastal side without the offshore side due to access limitations. For each location, 5 samples were collected from a 1-m radius and mixed to create a single representative sample of ~1 kg, ensuring comprehensive coverage of the site. Subsequently, the samples were transported in clean bags to the laboratory for geochemical analysis. Additionally, the total organic matter and pH values were measured. To achieve a stable weight, the samples were left to air-dry for 3 days at ambient temperature (about 27 °C). Subsequently, they pulverized. The size of the sediment samples (30 g) was examined. Both organic debris and carbonate were eliminated by treating each sample with diluted HCl and 15 % H_2O_2 (Song et al., 2023). Ternary diagrams (Folk, 1980) are used to analyze the textural classification of the sediment. This permits the sediment to be identified depending on its particle size, which can be gravel, sand, or mud (Ardila et al., 2023). For the sand and gravel fractions, wet sieving was utilized to calculate the sediment sample's grain size distribution; for the mud fraction, the pipette method was employed in accordance with Folk (Folk, 1980) methodology. The amount of organic stuff found in the samples (2 g) was ascertained by consecutive weight loss (single-stage LOI%) through igniting in a furnace set at 550 °C for about 6–8 h including drying and cooling time (Dean, 1974). The samples were weighed again using the procedure, to determine the weight % without any organic elements.

To eliminate the salinity, deionized water was used to wash the sediment samples. The heavy metals were measured using the smallest fractions (<63 μm) from the sediment samples, which involved air drying at room temperature, grinding, and screening. A solution of nitric acid (HNO_3), perchloric acid (HClO4), and hydrochloric acid (HCl) in a ratio of 5:1:1 (v/v/v) was used to digest the sediment samples (1 g) and to ensure complete dissolution of metals prior to ICP-OES analysis. The samples were then filtered to eliminate any leftover material. Nine metals (Ba, Co, Pb, Cu, Cr, Ni, Zn, V, and Fe) were extracted from the sediments under study using ICP-OES at the Desert Research Center, Cairo, Egypt, in accordance with Oregioni (Oregioni & Astone, 1984) method. External reference standards (SRM 2706 from NIST (USA) and Certipur from Merck Co. (Germany), that confirmed metal measurements' accuracy, with ICP-OES settings ensuring sensitivity and elemental recovery rates ranging from 90 % to 99 %.

2.3. Ecological, SQGs, and health indices

Five ecological indices: the enrichment factor (EF) (Zhang et al., 2017), contamination factor (Hakanson, 1980), index of geo-accumulation (I_{geo}) (Mueller, 1981), pollution load index (Tomlinson et al., 1980), Nemerow Pollution Index (NPI), and potential ecological risk index (PERI) (Hakanson, 1980), were calculated and used in this study. Three sediment quality guidelines were also utilized: modified hazard quotient (mHQ), toxic risk index (TRI) (Long & MacDonald, 1998), and mean effects range median quotient (MERMQ) (Long et al., 1995, 2000). Moreover, the non-carcinogenic hazard Index (HI) (Miletić et al., 2023; U.S. EPA, 2002), and total cancer risk (TCR) (U.S. EPA, 2002) were computed as human risk metrics. The Supplementary Material's Tables S1 and S2 revealed the indices' formulae and input information.

2.4. Radioactivity

The levels of Th, Ra, and K of the sixteen sediments that were collected from the Red Sea coastline's Abu Ghusun area (Fig. 1b). The

Nuclear Material Authority's (NMA) 76 × 76 mm sodium iodide [NaI (Tl)] analyzer was applied for detecting them. Sample preparation and the description of NaI detector including instrument operations, detection limits, and uncertainties (Supplementary Material). Quantifying the radiological emissions is crucial employing absorbed dose rates (D_{air}), radium equivalent activity (R_{aeq}), internal and external indices (H_{in} and H_{ex}), alpha and gamma index (I_{α} and I_{γ}) and indoor and outdoor effective doses (AED_{in} and AED_{out}) to perceive the radiological associated with the collected samples. The Raeq can be performed for estimating the danger criteria because of the internal alpha irradiation and external gamma exposure. Table S3 summarizes the methods required to evaluate these radiation risks and dosages.

2.5. Metals separation

To deduce if the studied coastal sediments contain any radioactive minerals or not, the samples were allowed to air dried and then quartered. Next, the heavy minerals from some samples were separated using the heavy liquid separation (bromoform) technique. Finally, the samples were magnetically fractionated using a Frantz isodynamic separator in accordance with their respective magnetic susceptibilities. In the NMA labs, the heavy minerals were selected using a binocular lens and identified with an Environmental Scanning Electron lens.

2.6. Statistical analysis

To evaluate the metal sources, analytical statistics comprising summary statistics (minimum, maximum, mean, standard deviation (SD), and coefficient of variance (CV), Pearson correlations, principal component analysis (PCA), and cluster analysis were done using Statgraphics software (version 18) (Reimann et al., 2008). In this study, one-variable analysis was utilized to detect whether the generated data came from a normal distribution using skewness and kurtosis.

3. Results and discussion

3.1. Sediment distribution

Table S4 presented the resluts of sediment grain size, type, pH, and total organic matter (TOM), while Table 1 summarizes the results and Fig. 2 illustrates their spatial distribution. The coastal sediments of Ab Ghusun were predominantly sandy (≈93.4 %), with minor mud (3.9 %) and alkaline (pH ≈ 8.4), and contained low to moderate TOM (2.5–6.5 %) (Ercegovac & Kostić, 2006), likely influenced by mangrove-derived organic debris along the shoreline (Fig. 1b). it is notes that pH, and TOM exhibited a spatial zigzag pattern with a northward increasing trnd (Fig. 2a). The results indicate that the skewness and kurtosis results of the sediment size, pH, and TOM were found to be in the predicted range (−2 to +2) (Table 1).

The coastal sediments of Abu Ghusun area are alkaline (pH = 8.4) and had medium ratios of TOM (up to 6.5 %) (Table 2), which possibly connected to the marshes of mangroves with lot of organic debris distributed along shoreline of the study area (Fig. S1d). Additionally, gravel (2.6 %) and mud (silt + clay%; 3.8 %) were the least in Abu Ghusun coastal sediments, while sand was the predominant fraction (93.4 %) (Table S3). Spatially, values of pH and organic matter in the examined sediment sites had a zigzag shape with an increasing from S1 to S16 (Fig. 2a). The middle sediments sites such as S6 have the greatest mud and gravel, and S11 has the highest ratios of sand, where a significant quantity of fluvial sediments from Wadi discharge that exist west of Abu Ghusun area were frequently flooding into the sea (Fig. 1b). Furthermore, S15 and S16 possess the greatest pH and TOM quantities, respectively (Fig. 1b and 2b).

3.2. Metals' concentrations and spatial pattern

Table S5 listed the nine metals that were analyzed in the Abu Ghusun sediments. Table 1 provides an overview the metals, and Fig. 3 exhibit their geographic abundance along the sampling sites (S1-16). The results show that the skewness and kurtosis of the nine heavy metals were found to be in the predicted range (−2 to +2) of a normal distribution (Table 1). For comparison with natural background, UCC values from Turekian and Wedepohl (1961) and Taylor and McLennan (1985) were used, while CSQG (2007) values were applied to assess potential ecological risks (Table 1). The decreasing order of the analyzed metals (mg/kg) as follows: Fe (48,927) > Ba (874.43) > V (160.81) > Cr (152.87) > Pb (121.93) > Zn (80.93) > Ni (77.5) > Cu (58.62) > Co (12) (Table 1). It is noticed that Abu Ghusun coastal sediments had higher contents of Ba, Pb, Cu, Cr, Ni, and V exceeding the CSQG and the crustal background (Taylor & McLennan, 1985) (Table 1). The diverse of basement rocks and tourism-related activities near the seashore might all be contributing factors to this metal enrichment (Al-Kahtany et al., 2023). In contrast, the examined metals, Co, Zn, and Fe, showed lower contents than those of the Canadian guideline (CSQG, 2007) and the earth crust background (Table 1). Spatially, the results showed that the middle sediment sites showed the highest metal contents in general (Fig. 3). Specifically, the largest contents of Ba, Co, Pb, Cu (Fig. 3a–d), and Zn (Fig. 3g) were revealed on the middle (S6-8, S10-11, and S15-16) and southern sites (S9 and S12-14) of Abu Ghusun area. While the largest contents of Cr, Ni (Fig. 3e–f), and V (Fig. 3h) were spatially concentrated on the northern (S1-5) and middle sites, with a decreasing northward trend (Fig. 3). These patterns suggest a combined influence of geogenic inputs from basement rocks and localized anthropogenic pressures, particularly from tourism and coastal activities. The middle sector appears to act as a sink for metal accumulation, possibly due to hydrodynamic trapping of fine sediments. The distinct north–south

Table 1
Summary statistics of the metals' contents (mg/kg) in the Abu Ghusun area.

n = 16	Gravel %	Sand %	Mud %	pH	TOM %	Ba	Co	Pb	Cu	Cr	Ni	Zn	V	Fe
Mean	2.66	93.44	3.89	8.47	4.33	**874.43**	12.00	**121.93**	58.62	**152.87**	**77.5**	80.93	**160.81**	48,927
Min	0.13	87.8	0.72	8.1	2.50	314	5	59	14	97	47	15	58	41,054
Max	4.95	99.15	7.25	8.92	6.50	1243	21	245	102	247	124	143	257	58,819
Median	2.57	93.95	3.75	8.46	4.30	1017.50	12	107	60.5	146	73.5	85	156.5	49,202
SD	1.53	3.37	2.02	0.24	1.33	292.62	4.87	53.45	31.33	41.48	21.35	38.26	60.31	4460
Skewness	−0.18	0.12	−0.11	0.49	0.24	−1.29	0.28	1.54	−0.27	1.14	1.25	−0.56	0.18	0.07
Kurtosis	−0.86	−0.51	−0.73	−0.60	−1.06	−0.38	−0.74	0.15	−1.21	0.13	0.09	−0.52	−0.90	0.61
CV	57.6	3.60	51.90	2.80	30.7	33.40	40	43.80	53.50	27.1	27.5	47.20	37.50	9.1
CSQG (2007)						750	40	70	63	64	50	200	130	–
Taylor and McLennan (1985)						425	25	12.5	55	100	75	70	135	56,300
Turekian and Wedepohl (1961)						580	19	20	45	90	68	95	130	47,200

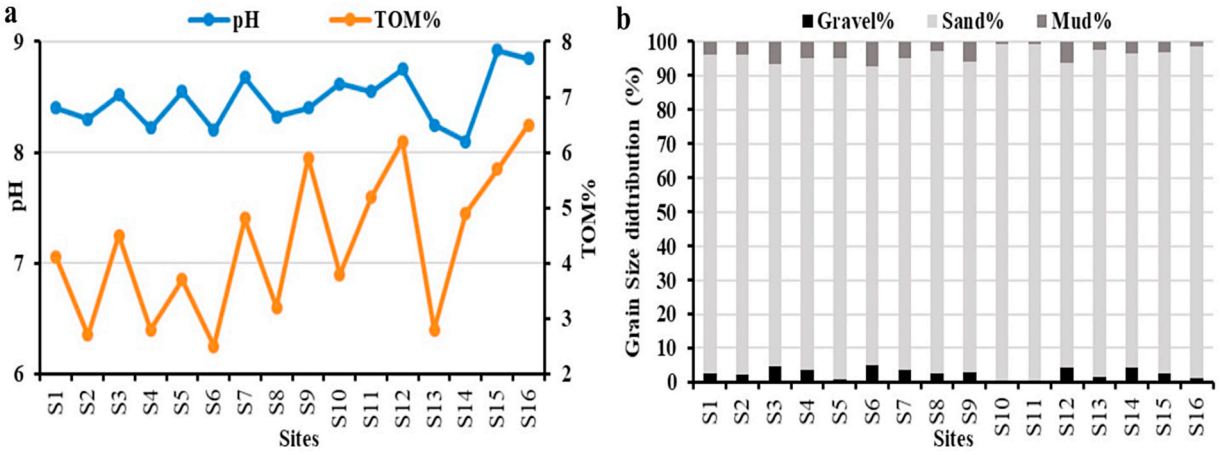

Fig. 2. Grain size (%) vs. a) pH, and b) total organic matter in Abu Ghusun area.

gradients also imply that wadi discharge and sediment transport dynamics play a key role in redistributing metals across the study area.

Mean metal values of Abu Ghusn coastal sediments were contrasted to the Egyptian and global sediments (Table 2). The comparison showed that the median levels of Ba, Pb, Cu, Cr, Ni, and V in Abu Ghusun sediments highly exceed those reported (Ba: 142–457 mg/kg; Pb: 0.84–29.4 mg/kg; Cu: 0.27–30.96 mg/kg; Cr: 10.62–86.1 mg/kg; Ni: 0.7–66 mg/kg; V: 6.67–142.8 mg/kg) in the Egyptian and global sediments (Al-Kahtany et al., 2023; Badawy et al., 2018; Nour et al., 2022; Lasheen, Mansour, et al., 2024; Yüksel et al., 2025) (Table 2). The mean levels of Co, Zn, and Fe in Abu Ghusun sediments were below those reported (Co: 17–71 mg/kg; Zn: 115–623 mg/kg; Fe: 65,966 mg/kg) in coastal sediments in Egypt and around the world (Fang & Chang, 2023) (Table 2).

3.3. Potential source of metals' pollution

The kurtosis and skewness ratios of the nine heavy metals in the Abu Ghusun sediments were found to be in the predicted range (−2 to +2) for a normal distribution, as seen in Table 1. A statistical metric called the coefficient of variance (CV) is employed to characterize the dispersion, or range, of data in relation to its median. When applied to metal concentrations in sediments, the CV helps to understand how consistently or variably metals are distributed across the study area. In this study, Fe (9.1 %) showed low variability (CV; <20 %) indicates that metal concentrations are relatively uniform across the sampling sites, suggesting natural geological processes (e.g., weathering of rocks, and mineral composition (Fig. 1c and Table 1). Ba, Co, Pb, Cr, Ni, Zn, and V showed moderate variability (CV; 20–50 %), which indicates a mix of natural (rock weathering) and anthropogenic sources (e.g., tourism-related activities). Copper (53.5 %) showed high variability (CV; >50 %) suggests potential localized sources of contamination (e.g., mineralization sites and mining activities west to the study area (Fig. 1c). Researchers identified high coefficients of correlation between a number of variables and heavy metals, including particle size, pH and organic matter content (Table 3 and Fig. S?). The study findings revealed significant correlations.

For example, Fig. 2 indicates that TOM% is negatively related to pH ($R^2 = 0.48$; $p < 0.01$) and is positively linked to Cu ($R^2 = 0.26$; $p < 0.05$). On the contrary, moderately good correlations were found between Co and Ba ($R^2 = 0.44$), Pb and Ba ($R^2 = 0.44$; $p < 0.01$) (Fig. 2), with Co ($R^2 = 0.31$) (Fig. 2), and with Zn ($R^2 = 0.43$) (Fig. 2). Moreover, no or weak correlations were found between Ba and Zn ($R^2 = 0.31$) (Fig. 2); Ni and Zn ($R^2 = 0.31$) (Fig. 2); and Cu and Fe ($R^2 = 0.31$) (Fig. 2 and Table 3). Parameters including pH, mud%, Cu, Cr, Ni, V and Fe did not find significant correlations with other metals that were analyzed (Table 3). Overall, the Pearson correlation results show that while Cu, Cr, Ni, V, and Fe may originate from several common sources, Co, Ba, Pb, Ni and Zn can be attributed to common sources (Table 3 and Fig. 2).

Five components were identified by the PCA findings for the metals in the Abu Ghusun sediments. According to Fig. 4a, the first PC1, which had positive significance loads of gravel%, mud%, and V, explained 31.48 % of the overall variance in the data. One common source might have been the inundation of debris into the Abu Ghusun shoreline from the Wadis west of the study sites (Fig. 1b). PC2 compensated for 16.94 % of data variance with high loadings of Pb, Cr, Ni, and Zn (Fig. 4a). This could be attributed to mixed sources of mining sites (e.g., Um Samiuki Cu, Pb, Zn, and Ag abandoned mining site, situated roughly 60 km to the west from Abu Ghusun shoreline, and tourism-related activities like tourist boats east of Abu Ghusun along the Red Sea shoreline (Al-Kahtany et al., 2023). According to Cyriac et al. (2021), the Pb in sediments is more likely from worn-out boat coatings and engine wear rather than leaded fuel. This conclusion is based on the global phase-out of leaded gasoline, particularly noting its prohibition in Egypt since 1996. Cr, Ni, and Zn primarily originate from antifouling paints, sacrificial anodes, and corrosion of boat materials. These sources contribute to the metal buildup in sediments along the shore, especially in areas with high tourist boat activity. In a similar vein, PC3, which had high loadings of Ba, Co, and Sand%, explained 14.7 % of the variation in the entire data set (Fig. 4a). According to literature, several metals show positive relationships with one another, suggesting that their sources are similar (Liang et al., 2018). PC4 demonstrated 10.2 % of the overall fluctuation in the data when positive loads of pH and TOM% were present. Meanwhile, PC5 accounted for4 8.35 % of the total fluctuation in the data when positive loads of Cu and Fe were present (Fig. 4a), indicating these components might have a common source. Evidently, the PCA results (Table 3 and Fig. 4) corroborated with the Pearson correlation results. Using the cluster analysis (HCA; Ward's-Euclidean method), the nine heavy metals, grain size, pH, and TOM detected in the coastal sediments of Abu Ghusun area were categorized into five groups (Fig. 4b). Co and Ba are in the first cluster, whereas TOM% and pH comprise the second cluster (Fig. 4b). Cu, Fe, and Sand% are included in the third cluster. Cr, Ni, and Mud% make up the fourth, whereas Pb, V, Zn, and Gravel% make up the fifth cluster. The PCA–HCA results suggest that Pb, Cr, Ni, and Zn are strongly linked to anthropogenic inputs, particularly abandoned mining activities (Um Samiuki site) and intensive boat operations (antifouling paints, sacrificial anodes, engine wear). In contrast, V, Ba, and Co align more with natural lithogenic inputs transported via Wadis. Cu and Fe clustering indicates mixed contributions, reflecting both natural sediment mineralogy and localized anthropogenic sources. As shown in Fig. 4, the cluster analysis confirmed the findings obtained from the PCA analysis.

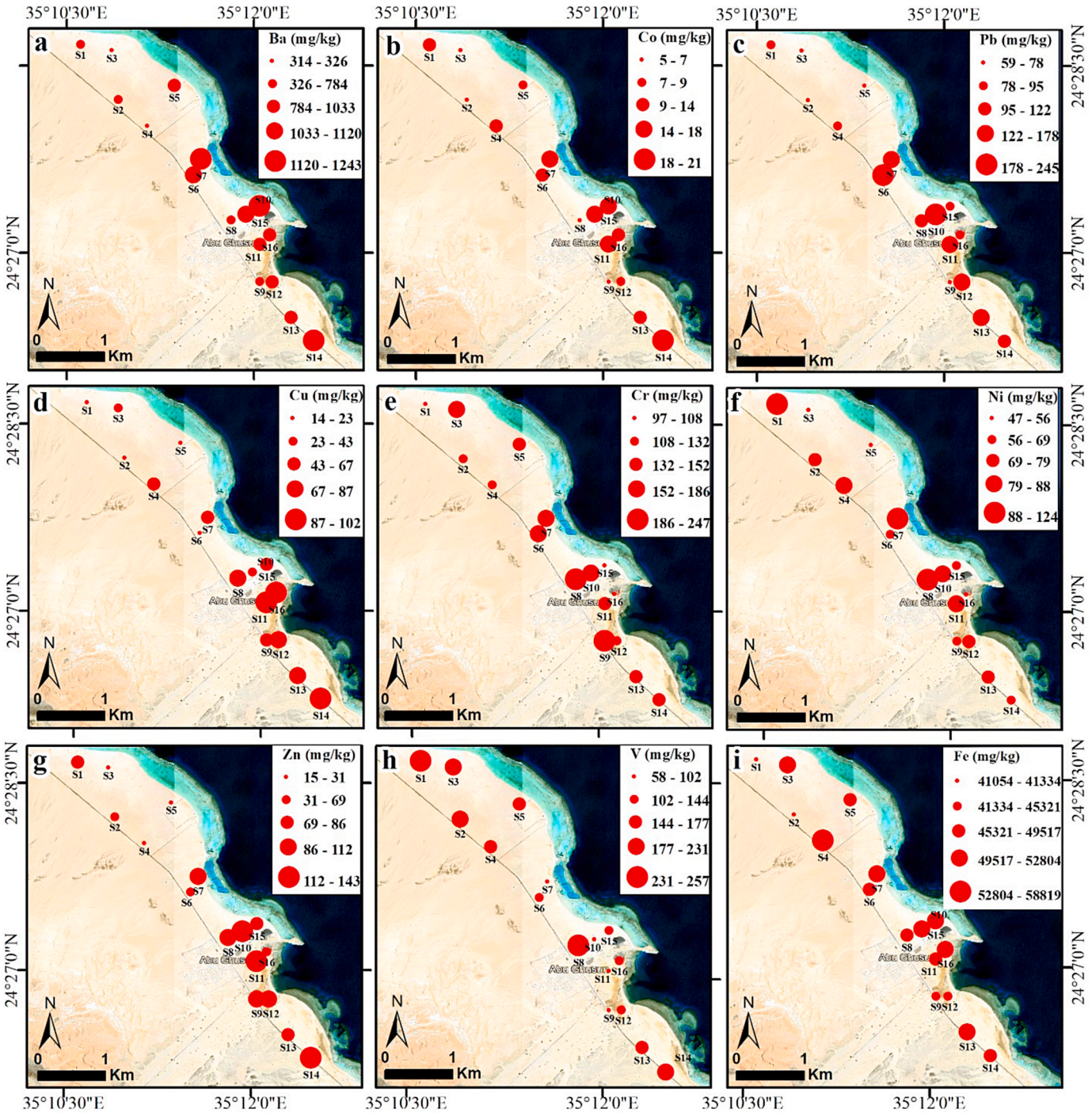

Fig. 3. Geographic pattern of metal contents (mg/kg) in Abu Ghusun sediments, Red Sea: a) Ba; b) Co; c) Pb; d) Cu; e) Cr; f) Ni; g) Zn; h) V; i) and Fe.

3.4. Metal pollution risk assessment

The determined enrichment factor measures of the metals under testing are illustrated in Table S6 and Fig. 5a in Abu Ghusun sediments. Table S5 and Fig. 5a reveal that the average EFs ranged from 0.19 to 9.7, with an average of 2.37. Pb and Ni exhibited the highest EFs (9.7 and 6.53, respectively), indicating considerable enhancement (EF = 5–20) based on the EF data (Fig. 5a). While the EFs of Co, Cr, Zn, and V showed minimal enhancement (EF = 1–2), the average EFs of Ba and Cu showed mild enhancement (EF = 2–5) (Abdelaal et al., 2024; Lasheen et al., 2025; Saleh, Lasheen, et al., 2025) (Fig. 5a; Table S1).

Table S7 and Fig. 5b display the calculated contamination factor (CF) results of examined metals in sediments of Abu Ghusun area. The sequence of average CFs was decreasing: Pb (4.88) > Ni (3.88) > Cu (2.25) > Ba (2.1) > V (1.61) > Cr (1.63) > Zn (1.23) > Co (1) > Fe (0.98) (Fig. 6b). While Ba, Co, Cu, Cr, Zn, and V reflect mild contamination ($3 \leq CF < 6$), Pb and Ni had the highest mean CF values, suggesting considerable contaminated sediments ($3 \leq CF < 6$) (Fig. 5b). Numerous elements, including basement rocks, ores, and tourist activities along the Red Sea beach, may have an impact on this metal pollution. Conversely, the average CF of Fe (0.98) revealed low contamination ($CF < 1$) (Abdelaal et al., 2024; Hakanson, 1980) (Fig. 5b).

Considering the nearby background reference numbers for the metals including iron are not available, the global average elemental

Table 2
The study's mean heavy metal concentrations (mg/kg) were contrasted others.

Location	Ba	Co	Pb	Cu	Cr	Ni	Zn	V	Fe	Reference
Abu Ghusun	874.43	12	121.93	58.62	152.87	77.50	80.93	160.81	48,927	This study
Red Sea coastline	171.84	4.81	4.89	7.70	53.84	15.37	27.55	29.78	14,562	Badawy et al. (2018)
W. El-Gemal outlet	–	1.24	2.57	0.47	–	2.44	6.74	–	4618	Al-Kahtany et al. (2023)
W. El-Gemal Island	–	2.05	0.84	0.31	–	0.70	3.40	–	1271	Lasheen, Mansour, et al. (2024)
Abu Minqar Island	–	2.34	1.19	0.27	–	0.76	2.89	–	921	Abdelaal et al. (2024)
Marsa Alam coast	–	1.83	2.23	1.94	10.62	6.82	28.83	–	1674	Farhat et al. (2022)
Gulf of Suez	–	7.40	2.78	1.66	8.98	5.58	3.96	–	540	(E Nour et al., 2022)
Aqaba coast	–	**18.81**	18.44	4.26	–	12.23	49.58	–	**50,395**	Mohammed et al. (2024)
Northeast coast	142	8	9	13	70	50	34	41	21,800	Vaezi and Lak (2023)
Lagoon lake	–	–	17.74	11.63	90.80	25.04	19.43	–	28,191	Yüksel et al. (2025)
Zhejiang coast	457.40	**17.17**	29.40	28.15	55.46	45	**115.87**	142.80	–	Zhao et al. (2023)
Mailiao coast	–	–	21.69	30.96	86.10	51.65	**174.12**	–	38,370	Fang and Chang (2023)

Table 3
Pearson correlations of Abu Ghusun area, Red Sea.

	Gravel%	Sand%	Mud%	pH	TOM%	Ba	Co	Pb	Cu	Cr	Ni	Zn	V	Fe
Gravel%	1													
Sand%	**0.93****	1												
Mud%	**0.80****	**−0.96****	1											
pH	−0.28	0.26	−0.23	1										
TOM%	−0.03	0.08	−0.11	**0.69****	1									
Ba	−0.23	0.28	−0.29	0.30	0.22	1								
Co	−0.16	0.34	−0.45	0.08	0.17	**0.66****	1							
Pb	−0.13	0.21	−0.25	0.02	−0.11	**0.62****	**0.55***	1						
Cu	−0.10	0.32	−0.45	0.17	**0.51***	0.35	0.38	0.17	1					
Cr	0.16	−0.19	0.20	−0.30	−0.20	0.05	−0.20	0.30	0.03	1				
Ni	0.01	0.11	−0.19	−0.14	−0.21	−0.02	0.01	0.25	0.12	0.36	1			
Zn	−0.18	0.34	−0.43	−0.01	0.23	**0.53***	0.45	**0.65****	0.44	0.38	0.46	1		
V	0.24	−0.15	0.07	−0.49	−0.48	−0.44	−0.31	−0.42	−0.24	−0.09	0.16	−0.26	1	
Fe	0.04	0.07	−0.14	0.08	−0.06	−0.01	0.36	0.10	0.35	−0.04	−0.09	−0.29	−0.19	1

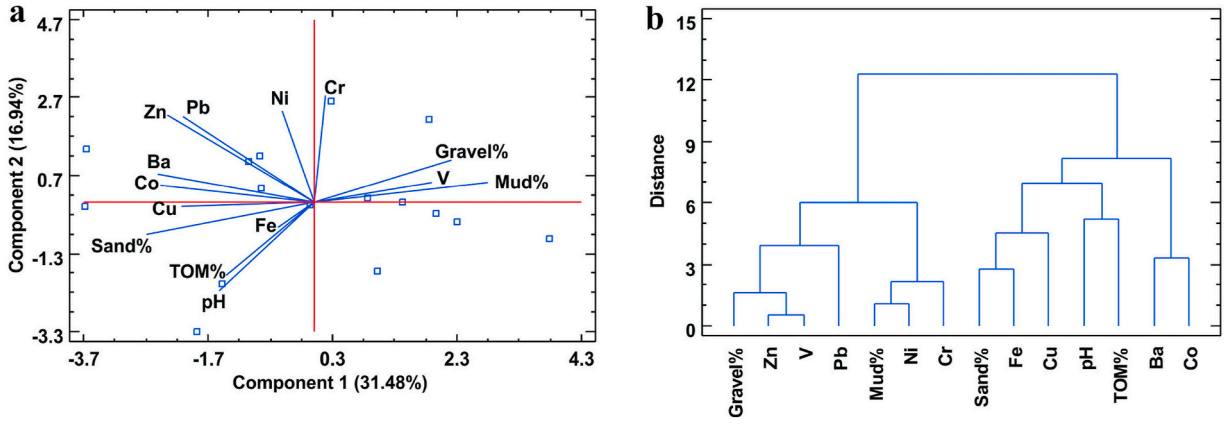

Fig. 4. a) PCA plot of the Abu Ghusun sediments. b) Dendrogram of the assessed metals.

concentrations in the upper crust (Turekian & Wedepohl, 1961) (Table 1), an approach frequently employed in current studies (Lasheen, Mansour, et al., 2024; Mostafa, 2002).

Fig. 5c and Table S8 display the computed geo-accumulation index (I_{geo}) of examined metals in sediments of Abu Ghusun area. The Igeo values of examined metals exhibited the following sequence: Fe (30.6) > Ba (17.8) > V (13.28) > Cr (13.27) > Zn (11.56) > Pb (10.87) > Ni (9.96) > Cu (9.71) > Co (6.46) (Table S8 and Fig. 5c). The I_{geo} values of all the metals that were tested varied from 5.32 to 30.87, with an average level of 13.72 (Fig. 5c) signifying highly polluted sediments (Fig. 5c). The iron content in coastal sediments of the Red Sea varies across different regions. According to Mahmoud et al. (Mohammed et al., 2024), the average iron content from the Red Sea coast (22,185 mg/kg) and Aqaba Gulf (50,395), and globally was 38,370–65,966 mg/kg in sediments of Taiwan and India, respectively (Table 2). These values indicate significant variations in iron concentrations across different parts of the Red Sea, which could be related to natural weathering of iron-rich rocks in the surrounding mining areas and anthropogenic activities (e.g., industrial discharges or shipping) (Abdelaal et al., 2024; Mohammed et al., 2024).

Table S7 and Fig. 5e present the PLI value of examined metals under investigation that were computed from the coastal sediments of Abu Ghusun. PLI values of metals had a range of 1.15–1.88 and a mean value of 1.52, demonstrating a progressive contamination (PLI >1) (Fig. 5e) (Hakanson, 1980). This suggests that the sediments are moderately polluted and not in pristine condition. The elevated PLI values also reflect the cumulative influence of both natural lithogenic inputs and localized anthropogenic activities along the coast.

Table S7 displays predicted Nemerow pollution metric (NPI) levels of metals in Abu Ghusun sediments. The NPI results in the metals under

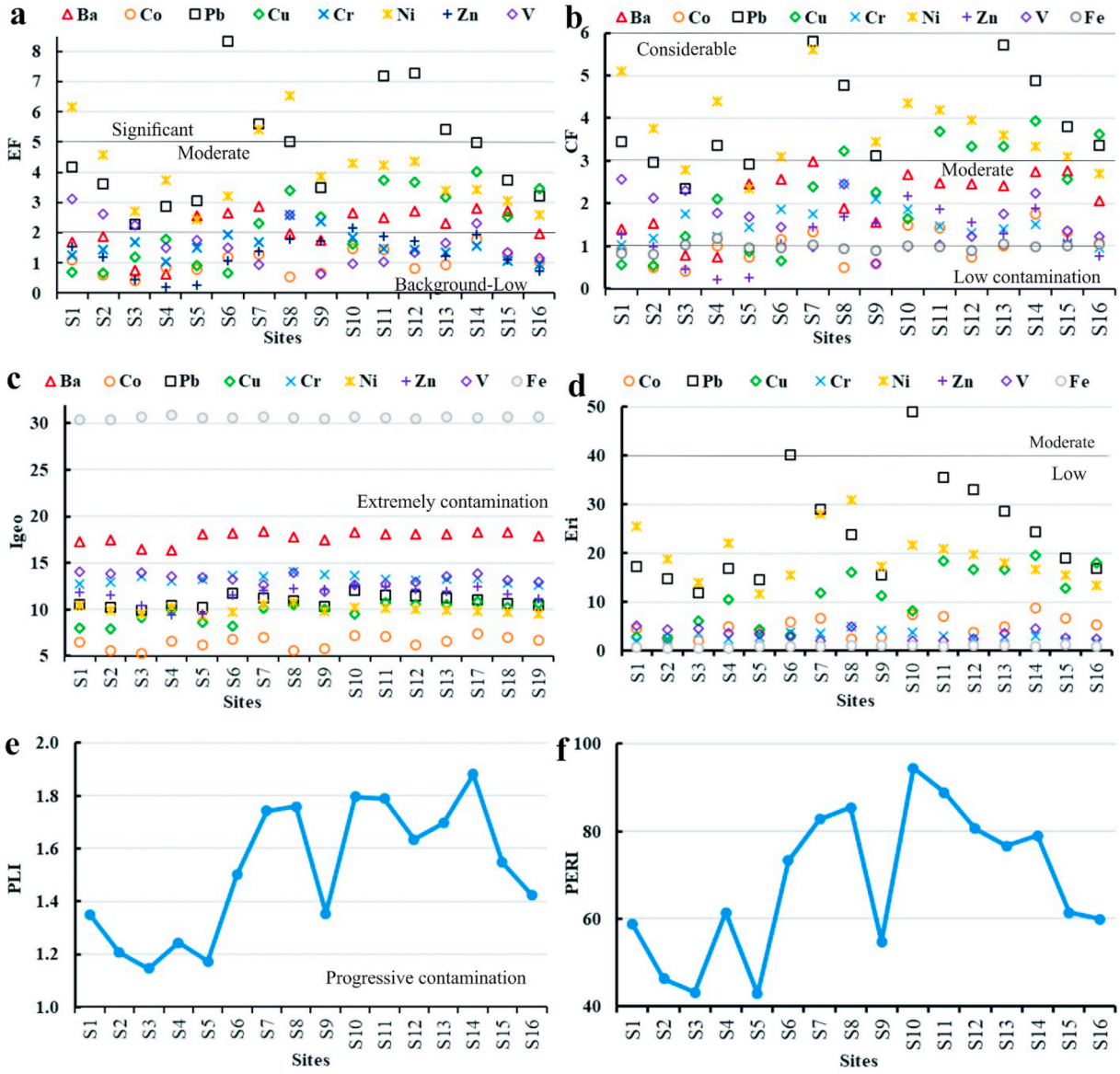

Fig. 5. a) The assessed enrichment metric: b) contamination metric; c) geo-accumulation index; d) ecological risk metric; e) pollution load index; and f) ecological risk factor.

investigation varied from 2.23 to 7.22 and a mean value of 4.02, suggesting highly polluted sediments (NPI >3), in accordance with the categorization of (Lasheen, Mansour, et al., 2024). These results highlight that metal pollution in the area is not only widespread but also unevenly distributed. The high NPI values further confirm that multiple metals contribute synergistically to the overall sediment contamination.

The potential ecological risk index (Er^i) and PERI were utilized to assess the metal levels in the Abu Ghusun sediments. The results are shown in Fig. 5d and f and Table S9. The metals under examination had Eri data exhibiting a median of 8.52 (Fig. 5d). Apart from Pb (sites S6 and S10), which showed moderate risk ($40 \leq Eri < 80$), all examined metals suggested low risk ($Eri < 40$) (Fig. 5d). Comparably, the study's examined metals' PERI values ranged from 42.86 to 94.5, with median 68.13, suggesting low risk ($PERI < 150$) (Hakanson, 1980) (Table S8 and Fig. 5f).

The estimated levels of mean effects range median quotient (MERMQ) as specified by sediment quality guidelines (SQGs) effects range-low (ERL) and effects range-median (ERM) (Long et al., 2000) of the studied metals in the Abu Ghusun (Table S10 and Fig. 6a). The comparison findings between the SQGs ERL, ERM, threshold effect level (TEL), probable effect level (PEL) (Long et al., 2000), and the contents of Pb, Cu, Cr, Ni, and Zn in sediments of Abu Ghusun area are shown in Table S11. It demonstrates that 8 sites, or 50 % of the total, elevated the ERM level of lead (110 mg/kg) and 56 % surpass the PEL level of lead (91.3 mg/kg). In a similar vein, 100 % of sediment sites are above the PEL values of Cr and Ni (90 and 36 mg/kg, respectively), whereas 56 % and 93 % of sites exceed the ERM limits of Cr and Ni (145 and 50 mg/kg, respectively). Moreover, Cu and Zn were below their corresponding ERL, ERM, TEL, and PEL values (Table S11). The mild/high risk ($0.51 < MERMQ \leq 1.5$) of the estimated MERMQ data of Pb, Cu, Cr, Ni, and Zn ranged from 0.55 to 1.18, with a mean value of 0.83 (Table S10 and Fig. 6a).

Table S12 and Fig. 7b and c exhibit the calculated toxic risk index (TRI) levels of Pb, Cu, Cr, Ni, and Zn in Abu Ghusun, in accordance to the SQGs TEL and PEL. The multi-element TRI levels of the sediment sites lies between 7.19 and 15.47 with median 10.86 (Fig. 6b), signifying a moderate toxic risk ($10 < TRI \leq 15$). Moreover, low toxic risk ($5 < TRI \leq 10$) was indicated by the largest TRI values of Ni (5.45), Cr (5.07), and Pb (5.3) (Zhang et al., 2017) (Fig. 6c).

The calculated modified hazard quotient (mHQ) of examined metals

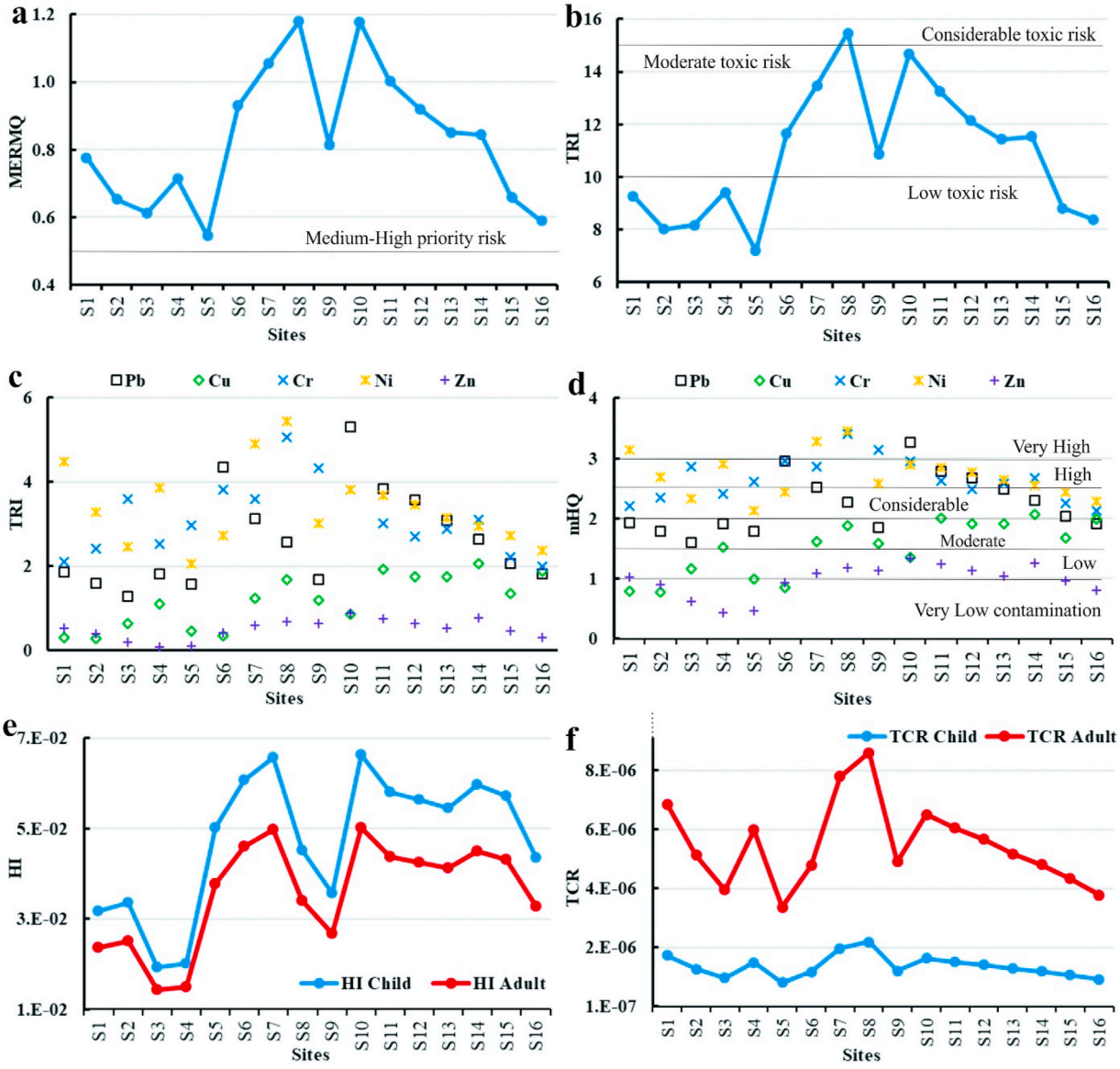

Fig. 6. a) The SQG values: a); b, c) TRI toxic index; d) Hazard quotient: e) Non-carcinogenic health index; and f) Carcinogenic risk index.

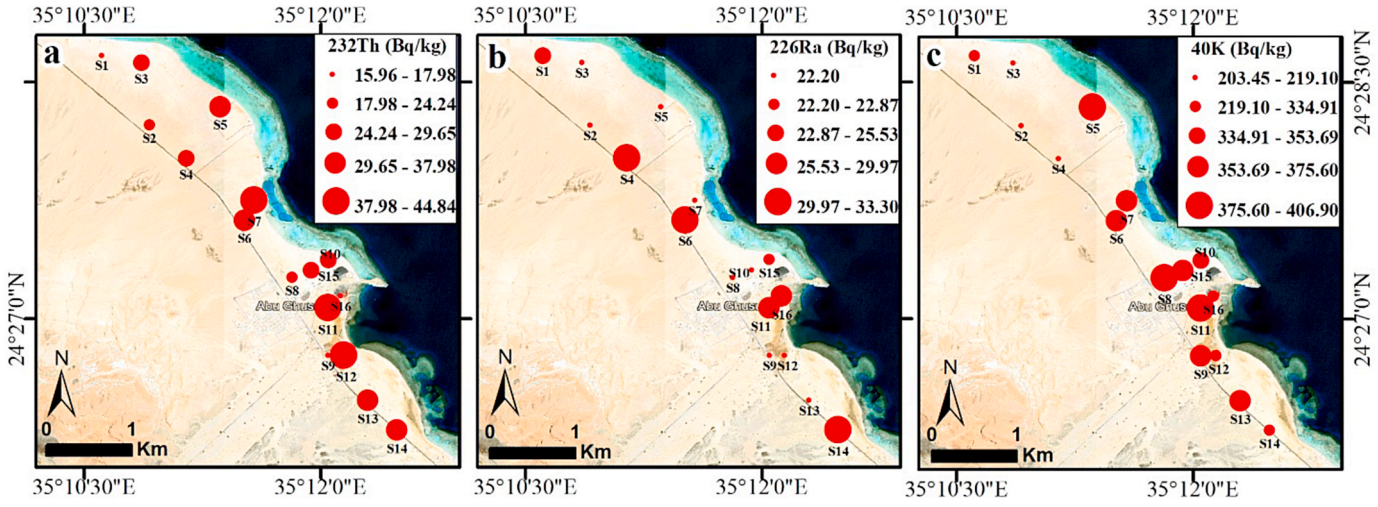

Fig. 7. Geographic distribution of the radionuclide's limits (Bq/kg) of ^{226}Ra (a), ^{232}Th (b), and ^{40}K (c) in Abu Ghusun sediments.

in Abu Ghusun sediments as displayed in Table S13 and Fig. 6d. The SQGs had a significant impact intensity, PEL, and TEL were utilized to obtain these values (Long et al., 1995; Macdonald et al., 1996). The mean metals' mHQ levels ranged from 0.43 to 3.46, with median of 2.02, signifying a significant level of contamination ($2.0 \leq$ mHQ <2.5) (Fig. 6d). In the sediments under investigation, the metals' mHQ values showed the following decreasing order: Ni (2.71) > Cr (2.66) > Pb (2.26) > Cu (1.51) > Zn (0.97) (Fig. 6d).

3.5. Appraisal of human health risks

The obtained non-carcinogenic health hazard index (HI) levels of heavy metals that were examined in the Abu Ghusun sediments are displayed in Table S14 and Fig. 6e. The hazard quotient (HQ), reference dose (RfD), and chronic daily intake (CDI_{Dermal}) (Table S2) of the metals under investigation were used to calculate the HI risk limits for adults and children (U.S. EPA, 2002). The largest levels of HQ_{Child} and HQ_{Adult} in sediments were discovered in Ba, as displayed in Table S12 (5.45×10^{-2} and 4.16×10^{-2}, respectively). Table S14 shows that the levels of HQ_{Adult} ranged from 8.2×10^{-6} to 4.16×10^{-2} with a mean value of 5.38×10^{-3}, whilst the HQ_{Child} data is in between $1.07 \times 10-5$ to 5.45×10^{-2}, with a mean level of 7.05×10^{-3}. According to Table S14, all metals have HQ values below the permissible limit (HQ < 1). Moreover, HI_{Child} levels lie between 2.13×10^{-4} and 6.83×10^{-2} with a median of 4.94×10^{-2}, whereas HI_{Adult} values were somewhat lower, displaying from 1.62×10^{-2} to 5.21×10^{-2} with median of 3.77×10^{-2} (Fig. 6e). The HI levels of examined metals in sediments of Abu Ghusun did not reveal any chronic hazards (HI < 1).

In Abu Ghusun sediments, total cancer risk (TCR) levels for adults and children are listed in Table S13 and Fig. 6f. TCR levels for Cd, Pb, and Ni were computed assuming the cancer risk (CR), cancer slope factor (CSF), and chronic daily intake (CDI_{Dermal}). The greatest values of CR_{Child} (2.08×10^{-6}) and CR_{Adult} (7.93×10^{-6}) were obtained in the Abu Ghusun sediments for Ni, followed by Pb and Cr (Table S15). All the CR values of the metals under investigation, however, are lower than the permissible threshold (1×10^{-6}) specified by U.S. EPA (U.S. EPA, 2002) (Table S15). Furthermore, the CR_{Child} levels of the metals under investigation ranged from 4.36×10^{-8} to 2.08×10^{-6} with median of 4.87×10^{-7}, while levels of CR_{Adult} ranged from 1.66×10^{-7} to 7.93×10^{-6} with a mean level of 1.86×10^{-6} (Table S15). TCR_{Child} levels of Pb, Cr, and Ni in sediments of Abu Ghusun displaying from 9.09×10^{-7} to 2.28×10^{-6} with a mean level of 1.46×10^{-6} (Fig. 6f), compared to more elevated values of TCR_{Adult}, which displaying from 3.47×10^{-6} to 8.7×10^{-6} with a mean value of 5.58×10^{-6} (Fig. 6f). TCR levels of Pb, Cr, and Ni in sediments of Abu Ghusun coastline were less than the permitted limit, which is 1×10^{-6} for a single element and 1×10^{-4} for multi-elements (Table S15 and Fig. 6f). Various malignancies can develop from prolonged exposure to small quantities of dangerous metals, including Pb, Cr, and Ni (Lasheen, Mansour, et al., 2024). Although individual CR values fall below permissible limits, their proximity to thresholds suggests possible concern under long-term exposure. The results highlight cumulative effects, particularly for vulnerable groups with chronic sediment contact or dietary exposure.

3.6. Radionuclide activity concentrations

The ^{226}Ra, ^{232}Th, and ^{40}K values of radionuclides in 16 coastal sediment samples were estimated and spatially distributed in Abu Ghusun area of the Red Sea coastline (Table 4 and Fig. 7). ^{226}Ra varied from 22.2 to 33.3 Bq/kg with a mean level of ±SD 25.43 ± 4.46, which is below the globally mean of 32 Bq/kg (Fig. 7b) (UNSCEAR, 2010; Zakaly et al., 2024).

In addition, all representative samples have ^{232}Th activity varies from 15.96 to 44.84 Bq/kg with mean ± SD 29.55 ± 8.87, which is below the global mean of 45 Bq/kg (Fig. 7a) (Lasheen et al., 2023; UNSCEAR, 2010). Notably, the value of ^{40}K is lower the worldwide limit (412 Bq/kg) (UNSCEAR, 2010), with mean ± SD values 337.06 ± 64.98 Bq/kg (Fig. 7c).

Table 4
^{226}Ra, ^{232}Th, and ^{40}K (Bq/kg) concentrations in Abu Ghusun coastal sediments.

Samples	^{232}Th	^{226}Ra	^{40}K
S1	16.16	25.53	313.00
S2	24.24	22.20	203.45
S3	25.78	22.20	219.10
S4	27.51	33.30	219.10
S5	37.98	22.20	406.90
S6	32.72	33.30	375.60
S7	41.21	22.20	366.21
S8	21.41	22.20	406.90
S9	15.96	22.20	375.60
S10	29.65	22.20	369.34
S11	44.84	29.97	406.90
S12	42.02	22.20	334.91
S13	33.94	22.20	375.60
S14	33.90	33.30	331.78
S15	27.51	22.87	353.69
S16	17.98	28.86	334.91
Min	15.96	22.20	203.45
Max	44.84	33.30	406.90
Mean	29.55	25.43	337.06
SD	8.87	4.46	64.98

We clarified that the relatively low radionuclide activity in the examined samples may be attributed either to the absence of nearby enriched sources, such as granitic rocks, or to the fact that the sediments themselves are derived from sources naturally poor in these radionuclides (Büyükuslu et al., 2018; Lasheen et al., 2025; Saleh, Lasheen, et al., 2025).

Notably, the collected samples have ordering pattern $^{40}K > ^{232}Th > ^{226}Ra$ of activity concentration (Table 4). The higher ^{40}K activity in theses samples can be ascribed to the abundance of leached feldspar from the host rocks certainly granitic rocks (Hanfi et al., 2022; Kumar et al., 2024). The silica component of the samples also influences ^{40}K availability to some degree.

By comparison the current results of ^{226}Ra, ^{232}Th, and ^{40}K activities with the previous global review levels as listed in Table S16. It is obvious that the current activities are less than those of Kumaun Himalaya, India (Ramola et al., 2011), Dois Rios beach, Brazil (Freitas & Alencar, 2004), Red Sea coast, Egypt (Harb, 2008), Aegean coast, Greece (Shahrokhi et al., 2020), Corbu beach, Romania ((Margineanu et al., 2013), and the global limit of (UNSCEAR, 2010), and close to those of the West coast, Thailand (Malain et al., 2010) (Table S16).

3.7. Radiological risk indices

An evaluation of radiological risks associated with Abu Ghusun sediments has been conducted using various indices (Table 5). The D_{air} index is utilized to assess gamma ray emissions at a distance exceeding 1 m from surface (Al-Mur et al., 2025; Lasheen et al., 2025; UNSCEAR, 2000, 2010). It varies from 34.23 to 59.84 with mean 44.77 ± 7.55 nGy h^{-1}, which lie within the globally safety (59 nGy h^{-1}) level (Akkurt & Günoğlu, 2014; Kumar et al., 2024; UNSCEAR, 2010). The Ra_{eq} refers to external and internal alpha particles and gamma-ray exposure dose. The calculated values lie within the permitted value (370 Bq/kg) (UNSCEAR, 2010), which have the mean 93.64 ± 15.83 Bq/kg. The AED_{out} and AED_{in} are used the D_{air} results, conversion factor of 0.7 Sv Gy^{-1}, indoor (0.8), and outdoor (0.2) occupancy number were applied to infer AED (O'Brien & Sanna, 1976). The computed mean AED_{out} data is 0.05 ± 0.01 mSv y^{-1}, which is below the permitted level (UNSCEAR, 2010) (70 μSvy^{-1}). Additionally, the average AED_{in} is 0.22 ± 0.04 mSvy^{-1}, which is below the permitted value (UNSCEAR, 2010) (0.41 μSvy^{-1}). The H_{in} & H_{ex} were computed to identify the radiation effect on human body (Ravisankar et al., 2015; UNSCEAR, 2010).

The values of H_{in} and H_{ex} for each collected samples are below unity

Table 5
Radiological parameters of Abu Ghusun coastal sediments.

Samples	Absorbed nGy h^{-1}	H_{in}	H_{ex}	I_α	I_γ	AEDout ($mSv\ y^{-1}$)	AEDin ($mSv\ y^{-1}$)	Ra_{eq}
S1	34.89	0.27	0.20	0.13	0.27	0.04	0.17	72.74
S2	34.23	0.26	0.20	0.11	0.26	0.04	0.17	72.53
S3	35.91	0.27	0.21	0.11	0.28	0.04	0.18	75.93
S4	41.84	0.33	0.24	0.17	0.32	0.05	0.21	89.51
S5	51.93	0.35	0.29	0.11	0.40	0.06	0.25	107.84
S6	51.89	0.38	0.29	0.17	0.40	0.06	0.25	109.02
S7	52.37	0.36	0.30	0.11	0.40	0.06	0.26	109.33
S8	40.90	0.29	0.23	0.11	0.32	0.05	0.20	84.15
S9	35.95	0.26	0.20	0.11	0.28	0.04	0.18	73.94
S10	44.81	0.31	0.25	0.11	0.35	0.05	0.22	93.04
S11	59.84	0.42	0.34	0.15	0.46	0.07	0.29	125.43
S12	51.59	0.35	0.29	0.11	0.40	0.06	0.25	108.07
S13	47.92	0.33	0.27	0.11	0.37	0.06	0.24	99.65
S14	50.83	0.38	0.29	0.17	0.39	0.06	0.25	107.32
S15	43.01	0.30	0.24	0.11	0.33	0.05	0.21	89.44
S16	38.45	0.30	0.22	0.14	0.30	0.05	0.19	80.36
Min	34.23	0.26	0.20	0.11	0.26	0.04	0.17	72.53
Max	59.84	0.42	0.34	0.17	0.46	0.07	0.29	125.43
Mean	44.77	0.32	0.25	0.13	0.34	0.05	0.22	93.64
SD	7.55	0.05	0.04	0.02	0.06	0.01	0.04	15.83

$D_{organs\ out}$ ($mSv\ y^{-1}$)							$D_{organs\ in}$ ($mSv\ y^{-1}$)						
Liver	Ovaries	Kidneys	Lungs	Bone Marrow	Testes	Entire Body	Liver	Ovaries	Kidneys	Lungs	Bone Marrow	Testes	Entire Body
0.02	0.02	0.03	0.03	0.03	0.04	0.03	0.08	0.10	0.11	0.11	0.12	0.14	0.12
0.02	0.02	0.03	0.03	0.03	0.03	0.03	0.08	0.10	0.10	0.11	0.12	0.14	0.12
0.02	0.03	0.03	0.03	0.03	0.04	0.03	0.08	0.10	0.11	0.11	0.12	0.14	0.12
0.02	0.03	0.03	0.03	0.04	0.04	0.03	0.09	0.12	0.13	0.13	0.14	0.17	0.14
0.03	0.04	0.04	0.04	0.04	0.05	0.04	0.12	0.15	0.16	0.16	0.18	0.21	0.18
0.03	0.04	0.04	0.04	0.04	0.05	0.04	0.12	0.15	0.16	0.16	0.18	0.21	0.18
0.03	0.04	0.04	0.04	0.04	0.05	0.04	0.12	0.15	0.16	0.16	0.18	0.21	0.18
0.02	0.03	0.03	0.03	0.03	0.04	0.03	0.09	0.12	0.12	0.13	0.14	0.16	0.14
0.02	0.03	0.03	0.03	0.03	0.04	0.03	0.08	0.10	0.11	0.11	0.12	0.14	0.12
0.03	0.03	0.03	0.04	0.04	0.05	0.04	0.10	0.13	0.14	0.14	0.15	0.18	0.15
0.03	0.04	0.05	0.05	0.05	0.06	0.05	0.14	0.17	0.18	0.19	0.20	0.24	0.20
0.03	0.04	0.04	0.04	0.04	0.05	0.04	0.12	0.15	0.16	0.16	0.17	0.21	0.17
0.03	0.03	0.04	0.04	0.04	0.05	0.04	0.11	0.14	0.15	0.15	0.16	0.19	0.16
0.03	0.04	0.04	0.04	0.04	0.05	0.04	0.11	0.14	0.15	0.16	0.17	0.20	0.17
0.02	0.03	0.03	0.03	0.04	0.04	0.04	0.10	0.12	0.13	0.14	0.15	0.17	0.15
0.02	0.03	0.03	0.03	0.03	0.04	0.03	0.09	0.11	0.12	0.12	0.13	0.15	0.13
0.02	0.02	0.03	0.03	0.03	0.03	0.03	0.08	0.10	0.10	0.11	0.12	0.14	0.12
0.03	0.04	0.05	0.05	0.05	0.06	0.05	0.14	0.17	0.18	0.19	0.20	0.24	0.20
0.03	0.03	0.03	0.04	0.04	0.05	0.04	0.10	0.13	0.14	0.14	0.15	0.18	0.15
0.00	0.01	0.01	0.01	0.01	0.01	0.01	0.02	0.02	0.02	0.02	0.03	0.03	0.03

(0.32 ± 0.05 and 0.25 ± 0.04, respectively), claiming that there aren't any serious health risks related with the collected samples (European Commission, 1999). I_α and I_γ have average levels of 0.13 ± 0.02 and 0.34 ± 0.06, respectively, which are below 1 (permitted value). It signifies that radiological hazards related to these sediments of Abu Ghusun area are negligible. D_{organs} can be applied to infer the amount of radiation that has accumulated in an individual's organs. The liver, ovaries, kidneys, lung, whole body, testes, bone, and marrow can be acquired with yearly (indoor and outdoor) effective dosages and conversion factors of 0.46, 0.58, 0.62, 0.64, 0.68, 0.69, and 0.82, respectively (O'Brien & Sanna, 1976). Notably, the $D_{organs\ in}$ levels are higher than those of $D_{organs\ out}$ and both indices are less than unity (permissible levels). Moreover, the liver's D_{organs}, both inside and outside the body, receive the minimal radiation exposure in relation to other tissues in humans. In contrast, the testes' indoor and outdoor components are exposed to the highest dose. Overall, several studies highlight that granitoid rocks are enriched in both trace metals (e.g., Ba, Pb, Ni) and naturally occurring radionuclides (Th, U, Ra, K) due to their mineralogical composition (UNSCEAR, 2000). Weathering and erosion of these rocks release both contaminants simultaneously into surrounding sediments. Hence, overlapping geological sources may explain the parallel occurrence of metals and radionuclides.

3.8. Mineralization

The separated heavy minerals that were drawn appling a binocular microscope and identified using ESEM are summarized in Fig. 8. The main separate minerals are garnet and leucoxene. Garnet reveals orange color with an equal grain under a binocular microscope. ESEM data of garnet grains show that they are almandine-rich (Fe = 22 %, Al = 11.3 %, Mg = 1.3 %, Ca = 4.3 %, and Mn = 5.3 %) (Fig. 8a). Leucoxene grain is a brown and granular alteration product of titanium minerals certainly ilmenite and/or titanite. ESEM data on leucoxene grains show that they are composed mainly of Fe = 27.3 %, Ti = 24.6 %, Mn = 1.8 %, Ca = 0.5 %. Al = 2.3 % (Fig. 8b).

3.9. Strengths and limitations

This study offers important strengths, as it provides the first comprehensive assessment of metal contamination and the associated ecological and human health risks in coastal sediments from Abu Ghusun, along the southern Egyptian Red Sea. However, several limitations should be acknowledged. Fieldwork and sampling (to a depth of ~10 cm) were conducted during a single campaign in June 2023, and sediment collection was restricted to the immediate coastline. Samples from beach deposits and the eastern offshore section of the study area could

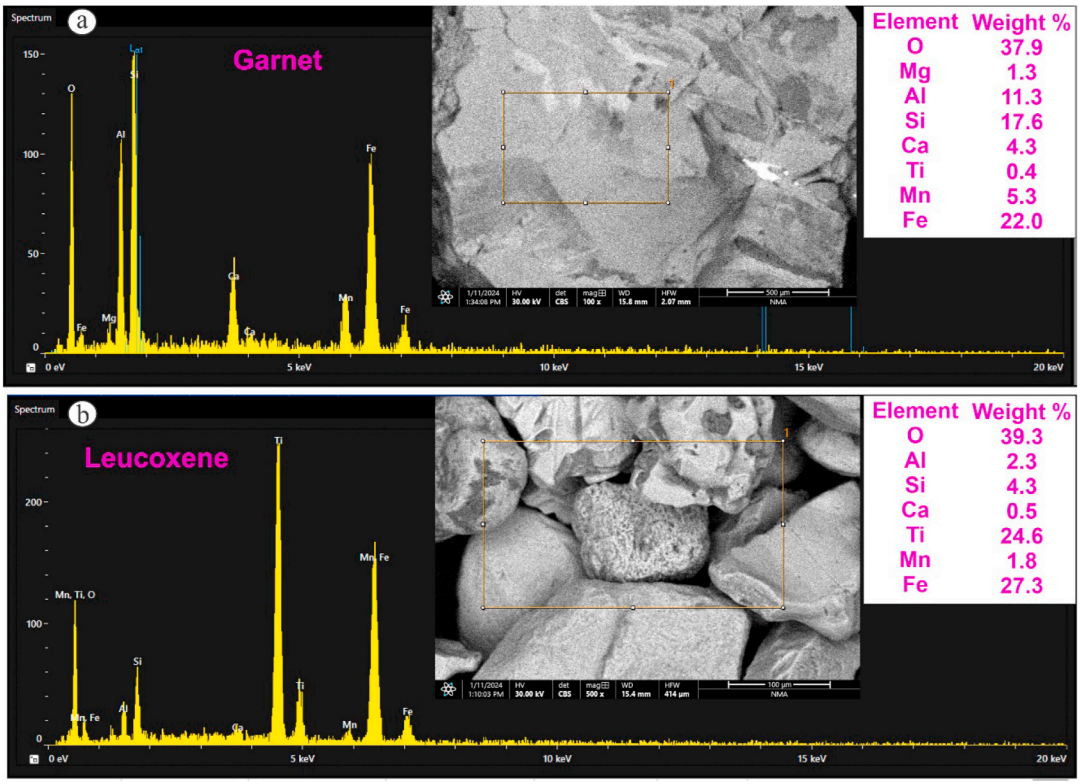

Fig. 8. ESEM analysis of Garnet (a), and Leucoxene (b) minerals.

not be obtained due to time, resources, and access limitations.

4. Conclusions

This study assessed nine heavy metals, their spatial distribution, and associated environmental and human health risks in 16 surface sediments from Abu Ghusun along the Red Sea coast. The sediments were alkaline, dominated by sand, and contained moderate organic matter. Metal concentrations followed the order: Fe (48,927) > Ba (874.43) > V (160.81) > Cr (152.87) > Pb (121.93) > Zn (80.93) > Ni (77.5) > Cu (58.62) > Co (12). Abu Ghusun sediments showed elevated Ba, Pb, Cu, Cr, Ni, and V, exceeding Canadian guidelines and crustal values, while Co, Zn, and Fe were lower. Spatially, Ba, Co, Pb, Cu, and Zn were enriched in the middle and southern sites, whereas Cr, Ni, and V peaked in the north and middle, decreasing northward.

Correlation and PCA analyses highlighted associations among metals and sediment properties, grouping Pb, Cr, Ni, and Zn as key contributors. EF, CF, and Igeo indicated moderate to high enrichment, with Pb and Ni being the most concerning. PLI (>1) and NPI (>3) confirmed progressive to high pollution, though risk indices (Er^i, PERI) suggested generally low ecological risk, with Pb posing the greatest threat. Toxicity and hazard indices indicated medium–high priority risk, especially for Ba and Ni in human health assessments.

Radiological analysis revealed mean activities of ^{232}Th, ^{226}Ra, and ^{40}K that are 12.1 ± 6.42, 24.53 ± 5.65, and 337.06 ± 64.98 Bq/kg, respectively, below global limits, with hazard indices (H_{in}, H_{ex}, H_{α}, and H_{γ}) reflecting negligible gamma radiation risk. The sediments also contained heavy minerals such as garnet and Ti-rich leucoxene. Overall, Abu Ghusun sediments are moderately to highly polluted by several metals, requiring attention to potential ecological and health impacts. The main isolated heavy minerals are garnet and titanium-rich leucoxene.

Future investigations should therefore incorporate long-term monitoring, a broader sampling strategy, including core and source materials, isotopic analyses (e.g., Pb), seasonal variations in hydrodynamics, biological interactions, and the development of remediation measures and policy recommendations.

CRediT authorship contribution statement

Ahmed Abdelaal: Writing – review & editing, Writing – original draft, Software, Investigation, Data curation. **Gehad M. Saleh:** Writing – review & editing, Methodology, Formal analysis, Conceptualization. **El Saeed R. Lasheen:** Writing – review & editing, Writing – original draft, Software, Data curation, Conceptualization. **Mabrouk Sami:** Writing – review & editing, Methodology, Funding acquisition. **Farrage M. Khaleal:** Writing – review & editing, Investigation, Funding acquisition. **Ioan V. Sanislav:** Writing – review & editing, Investigation, Funding acquisition, Formal analysis. **Fathy Abdalla:** Writing – review & editing, Supervision, Methodology, Funding acquisition.

Data availability Statement

All results are present within the text of the manuscript.

Ethical approval

No research with human beings has been carried out by the authors.

Funding

The authors extend their appreciation to the King Saud University for funding through the ongoing research funding program (ORF-2025-1120), King Saud University, Riyadh, Saudi Arabia.

Conflicts of interest

None.

Appendix A. Supplementary data

Supplementary data to this article can be found online at https://doi.org/10.1016/j.jrras.2025.101976.

References

Abdelaal, A., Lasheen, E. S. R., Mansour, A. M., Mohamed, A. W., Osman, M. R., Khaleal, F. M., Tahoon, M. A., & Al-Mur, B. A. (2024). Assessing the ecological and health risks associated with heavy metal pollution levels in sediments of Big Giftun and Abu Minqar Islands, East Hurghada, Red Sea, Egypt. *Marine Pollution Bulletin, 198*, Article 115930. https://doi.org/10.1016/j.marpolbul.2023.115930

Akkurt, I., & Günoğlu, K. (2014). Natural radioactivity measurements and radiation dose estimation in some sedimentary rock samples in Turkey. *Science and Technology of Nuclear Installations, 2014*, 1–6. https://doi.org/10.1155/2014/950978

Al-Kahtany, K., Nour, H. E., El-Sorogy, A. S., & Alharbi, T. (2023). Ecological and health risk assessment of heavy metals contamination in mangrove sediments, Red Sea coast. *Marine Pollution Bulletin, 192*, Article 115000. https://doi.org/10.1016/j.marpolbul.2023.115000

Al-Mur, B. A., Aljahdali, M. H., Almeelbi, T., & Lasheen, E. S. R. (2025). Spatial radionuclide distribution, mineralogy, and radiological evaluation of the Jeddah shoreline sediments, Red Sea, Saudi Arabia. *Environmental Monitoring and Assessment, 197*(5), 593. https://doi.org/10.1007/s10661-025-13986-8

Ardila, P. A. R., Alonso, R.Á., Valsero, J. J. D., García, R. M., Cabrera, F.Á., Cosío, E. L., & Laforet, S. D. (2023). Assessment of heavy metal pollution in marine sediments from southwest of Mallorca island, Spain. *Environmental Science and Pollution Research, 30*(7), 16852–16866. https://doi.org/10.1007/s11356-022-25014-0

Badawy, W. M., El-Taher, A., Frontasyeva, M. V., Madkour, H. A., & Khater, A. E. M. (2018). Assessment of anthropogenic and geogenic impacts on marine sediments along the coastal areas of Egyptian Red Sea. *Applied Radiation and Isotopes, 140*, 314–326. https://doi.org/10.1016/j.apradiso.2018.07.034

Büyükuslu, H., Özdemir, F. B., Öge, T.Ö., & Gökce, H. (2018). Indoor and tap water radon (222Rn) concentration measurements at Giresun University campus areas. *Applied Radiation and Isotopes, 139*, 285–291. https://doi.org/10.1016/j.apradiso.2018.05.027

CSQG. (2007). *Canadian Soil Quality Guidelines (CSQG) for the protection of environmental and human health: Summary tables*. Winnipeg, MB, Canada: Canadian Council of Ministers of the Environment (CCME), 2007; Updated September 2007.

Cyriac, M., Gireeshkumar, T. R., Furtado, C. M., Fathin, K. P. F., Shameem, K., Shaik, A., Vignesh, E. R., Nair, M., Kocherla, M., & Balachandran, K. K. (2021). Distribution, contamination status and bioavailability of trace metals in surface sediments along the southwest coast of India. *Marine Pollution Bulletin, 164*, Article 112042. https://doi.org/10.1016/j.marpolbul.2021.112042

Dean, W. E., Jr. (1974). Determination of Carbonate and organic matter in calcareous sediments and sedimentary rocks by loss on ignition: Comparison with other methods. *SEPM Journal of Sedimentary Research, 44*. https://doi.org/10.1306/74D729D2-2B21-11D7-8648000102C1865D

E Nour, H., Alshehri, F., Sahour, H., El-Sorogy, A. S., & Tawfik, M. (2022). Assessment of heavy metal contamination and health risk in the coastal sediments of Suez Bay, Gulf of Suez, Egypt. *Journal of African Earth Sciences, 195*, Article 104663. https://doi.org/10.1016/j.jafrearsci.2022.104663

Ercegovac, M., & Kostić, A. (2006). Organic facies and palynofacies: Nomenclature, classification and applicability for petroleum source rock evaluation. *International Journal of Coal Geology, 68*(1–2), 70–78. https://doi.org/10.1016/j.coal.2005.11.009

European Commission. (1999). Radiological protection principles concerning the natural radioactivity of building materials. Radiation Protection 112. *Directorate general environment. Nuclear safety and civil protection*. European Commission.

Fang, T.-H., & Chang, J.-R. (2023). The geochemical and environmental characteristics of trace metals in coastal sediment discharge off the Mailiao Industrial Zone of central Western Taiwan. *Water, 15*(2), 250. https://doi.org/10.3390/w15020250

Farhat, H. I., Gad, A., Saleh, A., & Abd El Bakey, S. M. (2022). Risks assessment of potentially toxic elements' contamination in the Egyptian Red Sea surficial sediments. *Land, 11*(9), 1560. https://doi.org/10.3390/land11091560

Folk, R. (1980). *Petrology of sedimentary rocks. Austin, Tex: Hemphill pub. Co, print*.

Freitas, A. C., & Alencar, A. S. (2004). Gamma dose rates and distribution of natural radionuclides in sand beaches—Ilha Grande, Southeastern Brazil. *Journal of Environmental Radioactivity, 75*(2), 211–223. https://doi.org/10.1016/j.jenvrad.2004.01.002

Hakanson, L. (1980). An ecological risk index for aquatic pollution control.a sedimentological approach. *Water Research, 14*(8), 975–1001. https://doi.org/10.1016/0043-1354(80)90143-8

Hanfi, M. Y., Abdel Gawad, A. E., Eliwa, H., Ali, K., Taki, M. M., Sayyed, M. I., Khandaker, M. U., & Bradley, D. A. (2022). Assessment of radioactivity in Granitoids at Nikeiba, Southeastern Desert, Egypt; radionuclides concentrations and radiological hazard parameters. *Radiation Physics and Chemistry, 200*, Article 110113. https://doi.org/10.1016/j.radphyschem.2022.110113

Harb, S. (2008). Natural radioactivity and external gamma radiation exposure at the coastal Red Sea in Egypt. *Radiation Protection Dosimetry, 130*(3), 376–384. https://doi.org/10.1093/rpd/ncn064

Khaleal, F. M., Tahoon, M. A., Saleh, G. M., Kamar, M. S., Zakaly, H. M. H., Zidan, I. H., Al-Mur, B. A., Alarif, S. S., & Lasheen, E. S. R. (2023). Dolphin-shaped island: Exploring the natural resources and radiological hazards of Wadi El Gemal Island. *Marine Pollution Bulletin, 194*, Article 115367. https://doi.org/10.1016/j.marpolbul.2023.115367

Kumar, N., Khyalia, B., Yadav, J., Singh, B., Gupta, V., Singh, P. P., Singh, H., & Dalal, R. (2024). Assessment of natural radioactivity in soil around Khetri copper belt of Rajasthan, India. *Journal of Radioanalytical and Nuclear Chemistry, 333*(6), 3185–3194. https://doi.org/10.1007/s10967-023-09301-9

Lasheen, E. S. R., Awad, H. A., Ene, A., Alarifi, S. S., Rashwan, M. A., Kawady, N. A., Issa, S. A. M., & Zakaly, H. M. H. (2023). Mineralogical constituents and radioactivity analysis of commercial granitic ornamental stones: Assessing suitability and radiation safety. *Journal of Radiation Research and Applied Sciences, 16*(3), Article 100618. https://doi.org/10.1016/j.jrras.2023.100618

Lasheen, E. S. R., Mansour, A. M., Mohamed, A. W., Osman, M. R., Khaleal, F. M., Tahoon, M. A., Alarifi, N., Jordan, G., & Abdelaal, A. (2024). Assessing the heavy metals in surface sediments of wadi El-Gemal Island, Red Sea, Egypt: Pollution levels, sources, and associated risks. *Water, Air, & Soil Pollution, 235*(7), 461. https://doi.org/10.1007/s11270-024-07273-4

Lasheen, E. S. R., Saleh, G. M., Al-Mur, B. A., & Abdelaal, A. (2025). Assessing the radioactive properties and environmental risks of Hankorab sediments on the Red Sea coast. *Environmental Earth Sciences, 84*(14), 420. https://doi.org/10.1007/s12665-025-12418-7

Lasheen, E. S. R., Sami, M., Hegazy, A. A., Arman, H., Sanislav, I. V., Ahmed, M. S., & Rashwan, M. A. (2024). Petrological characteristics and physico-mechanical properties of dokhan volcanics for decorative stones and building material applications. *Buildings, 14*(11), 3418. https://doi.org/10.3390/buildings14113418

Liang, B., Qian, X., Peng, S., Liu, X., Bai, L., Cui, B., & Bai, J. (2018). Speciation variation and comprehensive risk assessment of Metal(loid)s in surface sediments of intertidal zones. *International Journal of Environmental Research and Public Health, 15*(10), 2125. https://doi.org/10.3390/ijerph15102125

Long, E. R., & MacDonald, D. D. (1998). Recommended uses of Empirically Derived, Sediment Quality Guidelines for marine and estuarine ecosystems. *Human and Ecological Risk Assessment: An International Journal, 4*(5), 1019–1039. https://doi.org/10.1080/10807039891284956

Long, E. R., MacDonald, D. D., Severn, C. G., & Hong, C. B. (2000). Classifying probabilities of acute toxicity in marine sediments with empirically derived sediment quality guidelines. *Environmental Toxicology and Chemistry, 19*(10), 2598–2601. https://doi.org/10.1002/etc.5620191028

Long, E. R., Macdonald, D. D., Smith, S. L., & Calder, F. D. (1995). Incidence of adverse biological effects within ranges of chemical concentrations in marine and estuarine sediments. *Environmental Management, 19*(1), 81–97. https://doi.org/10.1007/BF02472006

Macdonald, D. D., Carr, R. S., Calder, F. D., Long, E. R., & Ingersoll, C. G. (1996). Development and evaluation of sediment quality guidelines for Florida coastal waters. *Ecotoxicology, 5*(4), 253–278. https://doi.org/10.1007/BF00118995

Malain, D., Regan, P. H., Bradley, D. A., Matthews, M., Santawamaitre, T., & Al-Sulaiti, H. A. (2010). Measurements of NORM in beach sand samples along the Andaman coast of Thailand after the 2004 tsunami. *Nuclear Instruments and Methods in Physics Research Section A: Accelerators, Spectrometers, Detectors and Associated Equipment, 619*(1–3), 441–445. https://doi.org/10.1016/j.nima.2009.11.047

Margineanu, R. M., Duliu, O. G., Blebea-Apostu, A. M., Gomoiu, C., & Bercea, S. (2013). Environmental dose rate distribution along the Romanian Black Sea Shore. *Journal of Radioanalytical and Nuclear Chemistry, 298*(2), 1191–1196. https://doi.org/10.1007/s10967-013-2545-4

Miletić, A., Lučić, M., & Onjia, A. (2023). Exposure factors in health risk assessment of heavy Metal(loid)s in soil and sediment. *Metals, 13*(7), 1266. https://doi.org/10.3390/met13071266

Mohammadi, A. A., Zarei, A., Majidi, S., Ghaderpoury, A., Hashempour, Y., Saghi, M. H., Alinejad, A., Yousefi, M., Hosseingholizadeh, N., & Ghaderpoori, M. (2019). Carcinogenic and non-carcinogenic health risk assessment of heavy metals in drinking water of Khorramabad, Iran. *MethodsX, 6*, 1642–1651. https://doi.org/10.1016/j.mex.2019.07.017

Mohammed, A. H., Khalifa, A. M., Mohamed, H. M., Abd El-Wahid, K. H., & Hanafy, M. H. (2024). Assessment of heavy metals at mangrove ecosystem, applying multiple approaches using in-situ and remote sensing techniques, Red Sea, Egypt. *Environmental Science and Pollution Research, 31*(5), 8118–8133. https://doi.org/10.1007/s11356-023-31625-y

Mostafa, G. A. (2002). Monitoring of polycyclic aromatic hydrocarbons in seafoods from Lake Timsah. *International Journal of Environmental Health Research, 12*(1), 83–91. https://doi.org/10.1080/09603120120110086

Mueller, G. (1981). *Die Schwermetallbelastung der sedimente des Neckars und seiner Nebenflusse: Eine Bestandsaufnahme. CHEMIKER ZTG, 105* pp. 157–164).

O'Brien, K., & Sanna, R. (1976). The distribution of absorbed dose-rates in humans from exposure to environmental gamma rays. *Health Physics, 30*.

Oregioni, B., & Astone, S. (1984). *The determination of selected trace metals in marine sediments by flameless/flame-atomic absorption spectrophotometry*. IAEA Monaco Laborator [Internal].

Ramola, R. C., Choubey, V. M., Prasad, G., Gusain, G. S., Tosheva, Z., & Kies, A. (2011). Radionuclide analysisin the soil of Kumaun Himalaya, India, using gamma ray spectrometry. *Current Science, 100*(6), 6–25.

Ravisankar, R., Chandramohan, J., Chandrasekaran, A., Prince Prakash Jebakumar, J., Vijayalakshmi, I., Vijayagopal, P., & Venkatraman, B. (2015). Assessments of radioactivity concentration of natural radionuclides and radiological hazard indices in sediment samples from the East coast of Tamilnadu, India with statistical approach. *Marine Pollution Bulletin, 97*(1–2), 419–430. https://doi.org/10.1016/j.marpolbul.2015.05.058

Reeves, R. L. (1977). Comparison of triazolam, flurazepam, and placebo as hypnotics in geriatric patients with insomnia. *Journal of Clinical Pharmacology, 17*(5–6), 319–323. https://doi.org/10.1002/j.1552-4604.1977.tb04611.x

Reimann, C., Filzmoser, P., Garrett, R. G., & Dutter, R. (2008). In *Statistical data analysis explained: Applied environmental statistics with R* (1st ed.). Wiley. https://doi.org/10.1002/9780470987605.

Saleh, G. M., Kamar, M. S., Khaleal, F. M., Azer, M. K., Nasr, T., & Lasheen, E. S. R. (2025). Petrogenesis and tectonic evolution of tourmaline- bearing leucogranites, Sikait area, Southeastn desert of Egypt utilizing mineralogical and bulk rock analysis. *Scientific Reports, 15*(1), Article 20191. https://doi.org/10.1038/s41598-025-06155-x

Saleh, G. M., Lasheen, E. S. R., Foi, M., Abdalla, F., & Abdelaal, A. (2025). Assessment of radioactivity and heavy metal pollution levels in the coastal sediments in the Red Sea Region of Sharm El Luli, Egypt. *Water, Air, & Soil Pollution, 236*(5), 319. https://doi.org/10.1007/s11270-025-07962-8

Saralioglu, E., & Vatandaslar, C. (2022). Land use/land cover classification with Landsat-8 and Landsat-9 satellite images: A comparative analysis between forest- and agriculture-dominated landscapes using different machine learning methods. *Acta Geodaetica et Geophysica, 57*(4), 695–716. https://doi.org/10.1007/s40328-022-00400-9

Shahrokhi, A., Adelikhah, M., Chalupnik, S., Kocsis, E., Toth-Bodrogi, E., & Kovács, T. (2020). Radioactivity of building materials in Mahallat, Iran – An area exposed to a high level of natural background radiation – Attenuation of external radiation doses. *Materiales de Construcción, 70*(340), 233. https://doi.org/10.3989/mc.2020.03820

Song, X., Dong, J., Wang, H., Xie, H., Yu, Y., Geng, L., Yuan, Z., & Du, Y. (2023). Factors influencing the distribution of organic carbon in four different coastal sedimentary environments. *Journal of Soils and Sediments, 23*(3), 1539–1551. https://doi.org/10.1007/s11368-022-03423-5

Taylor, S. R., & McLennan, S. M. (1985). *The continental crust: Its composition and evolution*.

Tomlinson, D. L., Wilson, J. G., Harris, C. R., & Jeffrey, D. W. (1980). Problems in the assessment of heavy-metal levels in estuaries and the formation of a pollution index. *Helgolaender Meeresuntersuchungen, 33*(1–4), 566–575. https://doi.org/10.1007/BF02414780

Turekian, K. K., & Wedepohl, K. H. (1961). Distribution of the elements in some major units of the Earth's crust. *Geological Society of America Bulletin, 72*(2), 175. https://doi.org/10.1130/0016-7606(1961)72[175:DOTEIS]2.0.CO;2

UNSCEAR. (2000). In *Sources and effects of ionizing radiation: United Nations Scientific Committee on the Effects of Atomic Radiation: UNSCEAR 2000 report to the General Assembly, with scientific annexes*. United Nations.

UNSCEAR. (2010). In *Sources and effects of ionizing radiation: United Nations Scientific Committee on the Effects of Atomic Radiation: UNSCEAR 2008 report to the General Assembly, with scientific annexes*. United Nations.

U.S. EPA. (2002). *National recommended water quality criteria*. US Environmental Protection Agency, Office of Water.

Vaezi, A., & Lak, R. (2023). Sediment texture, geochemical variation, and ecological risk assessment of major elements and trace metals in the sediments of the Northeast Persian Gulf. *Minerals, 13*(7), 850. https://doi.org/10.3390/min13070850

Yüksel, B., Ustaoğlu, F., Topaldemir, H., Yazman, M. M., & Tokatlı, C. (2025). Unveiling the nutritional value and potentially toxic elements in fish species from Miliç Wetland, Türkiye: A probabilistic human health risk assessment using Monte Carlo simulation. *Marine Pollution Bulletin, 211*, Article 117417. https://doi.org/10.1016/j.marpolbul.2024.117417

Zakaly, H. M. H., Awad, H. A., Lasheen, E. S. R., Issa, S. A. M., Elsaman, R., Khandaker, M. U., Al-awah, H., Fathy, D., & Sami, M. (2024). Radiometric and petrographic characterization of El-Yatima granite: Evaluating radiological risks and mineralogical features. *Radiation Physics and Chemistry, 224*, Article 111992. https://doi.org/10.1016/j.radphyschem.2024.111992

Zhang, F., Sun, X., Zhou, Y., Zhao, C., Du, Z., & Liu, R. (2017). Ecosystem health assessment in coastal waters by considering spatio-temporal variations with intense anthropogenic disturbance. *Environmental Modelling & Software, 96*, 128–139. https://doi.org/10.1016/j.envsoft.2017.06.052

Zhao, Z., Liu, Q., Liao, Y., Yu, P., Tang, Y., Liu, Q., Shi, X., Shou, L., Zeng, J., Chen, Q., & Chen, J. (2023). Ecological risk assessment of trace metals in sediments and their effect on benthic organisms from the south coast of Zhejiang province, China. *Marine Pollution Bulletin, 187*, Article 114529. https://doi.org/10.1016/j.marpolbul.2022.114529